LANGMUIR

pubs.acs.org/Langmuir Article

Stabilization of Lipid Membranes through Partitioning of the Blood Bag Plasticizer Di-2-ethylhexyl phthalate (DEHP)

Renée-Claude Bider,[⊥] Telmah Lluka,[⊥] Sebastian Himbert, Adree Khondker, Syed M. Qadri, William P. Sheffield, and Maikel C. Rheinstädter*

Cite This: *Langmuir* 2020, 36, 11899–11907 Read Online

ABSTRACT: The safe storage of blood is of fundamental importance to health care systems all over the world. Currently, plastic bags are used for the collection and storage of donated blood and are typically made of poly(vinyl chloride) (PVC) plasticized with di-2-ethylhexyl phthalate (DEHP). DEHP is known to migrate into packed red blood cells (RBC) and has been found to extend their shelf life. It has been speculated that DEHP incorporates itself into the RBC membrane and alters membrane properties, thereby reducing susceptibility to hemolysis and morphological deterioration. Here, we used high-resolution X-ray diffraction and molecular dynamics (MD) simulations to study the interaction between DEHP and model POPC lipid membranes at high (9 mol %) and low (1 mol %) concentrations of DEHP. At both concentrations, DEHP was found to spontaneously partition into the bilayer. At high concentrations, DEHP molecules were found to aggregate in the aqueous phase before inserting as clusters into the membrane. The presence of DEHP in the bilayers resulted in subtle, yet statistically significant, alterations in several membrane properties in both the X-ray diffraction experiments and MD simulations. DEHP led to (1) an increase of membrane width and (2) an increase in the area per lipid. It was also found to (3) increase the deuterium order parameter, however, (4) decrease membrane orientation, indicating the formation of thicker, stiffer membranes with increased local curvature. The observed effects of DEHP on lipid bilayers may help to better understand its effect on RBC membranes in increasing the longevity of stored blood by improving membrane stability.

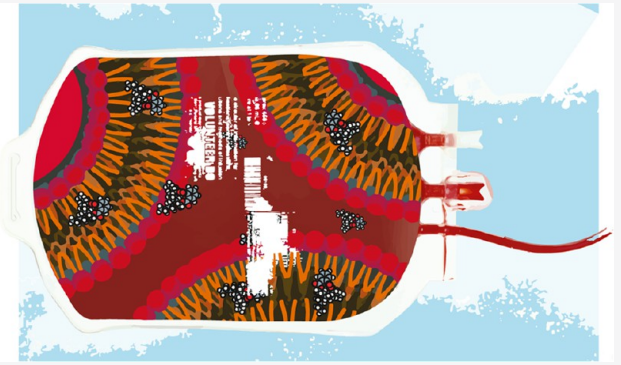

INTRODUCTION

The blood bag was introduced as a solution to a long-standing medical problem during wartime to safely perform blood transfusions. It revolutionized medicine, providing a portable and sterile storage solution and saving millions of lives. Today, blood bags are primarily composed of poly(vinyl chloride) (PVC) compounded with 30−40 wt % di(2-ethylhexyl)-phthalate (DEHP),[1] a plasticizer used to improve the bags' flexibility and durability. PVC-DEHP blood bags are particularly favored due to their unmatched sturdiness and resistance to damaging environmental factors, such as extreme temperatures or abrasion.[2] This blend also has a low cost of production due to its weldability and stability during steam sterilization, allowing for single-use bags.[3] Overall, PVC-DEHP blood bags combine many desirable properties, leading to their widespread use in the health care industry since their introduction in the 1950s.

However, recent *in vitro* and *in vivo* studies using murine models have shown that DEHP can produce toxic effects in multiple areas, such as the kidneys, reproductive tract organs,[4] and lungs,[5] in addition to hindering the function of Na^+/K^+ ATPase in the kidneys, brain, and red blood cells (RBCs).[6] Due to its lipophilic structure, DEHP is known to migrate from the PVC polymer matrix into packed red blood cells (RBC),[7,8] as illustrated in Figure 1. DEHP (15−83.2 μg/mL) was detected in PVC blood bags after 20 days of storage and 7.4−36.1 μg/mL of DEHP was found in irradiated RBC concentrate products.[9] The Scientific Committee on Emerging and Newly Identified Health Risks (SCENIHR) deemed that some medical procedures put patients at risk for prolonged DEHP exposure above the recommended dose, including exchange transfusion of blood in neonates and massive blood transfusions. Additionally, total parenteral nutrition, extracorporeal membrane oxygenation (ECMO) in neonates and adults, and hemodialysis put patients at risk of extreme DEHP

Received: July 3, 2020
Revised: September 9, 2020
Published: September 9, 2020

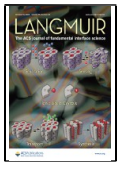

https://dx.doi.org/10.1021/acs.langmuir.0c01964
Langmuir 2020, 36, 11899−11907

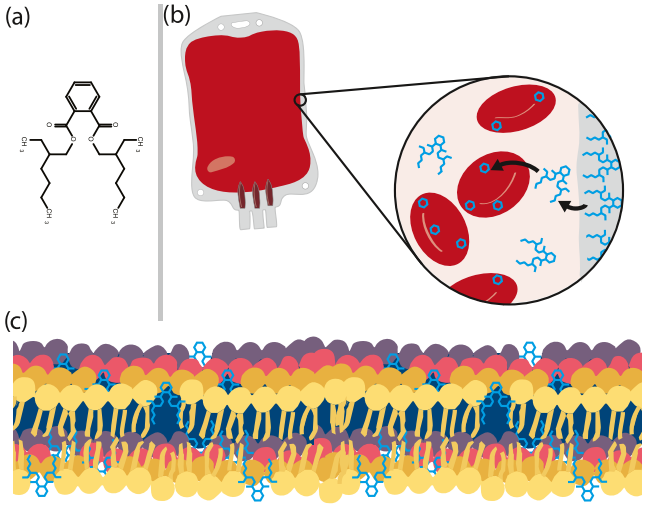

Figure 1. DEHP is a lipophilic plasticizer used in PVC blood bags (a). It is known to leach into stored blood and incorporates itself into its various components, including RBCs (b). DEHP has been shown to reduce hemolysis and cell deterioration. This was speculated to occur through active alteration of the cell's morphology after integrating itself into the RBC membrane, thereby increasing membrane stability (c).

exposure in blood.[10] However, efforts to replace DEHP with a less toxic alternative were unsuccessful due to its unique ability to extend the shelf life of packed RBCs by preventing morphological deterioration and hemolysis.[11,12]

Despite its widespread use in health care and its associated concerns, little is known about the exact interaction between DEHP and RBCs and their resulting effects. A study of the effects of DEHP on the RBC membrane composition by Almizraq et al.[13] found that blood stored for 49 days had a disproportionate decrease of phospholipids over time compared to cholesterol, leading to speculation that the significant loss of phospholipids might stabilize RBC membranes by reducing deformability. In a recent study by Melzak et al.,[14] DEHP was shown to counteract deleterious storage-related morphology changes, as well as induce the formation of stomatocytes. Three mechanisms by which this can occur were proposed: DEHP could remove lipids from the outer leaflet of the membrane, DEHP could induce lipid flip-flop, or DEHP could insert into the RBC membrane and increase the area per lipid.

In this study, we combined high-resolution X-ray diffraction and molecular dynamics (MD) computer simulations to collect molecular level information about the interaction between DEHP and model POPC lipid membranes. RBC membranes contain about 55 lipid species, with PC lipids, PE lipids, sphingomylin, and cholesterol, making up the largest part of the membrane. Though these four classes represent near equal proportions of the membrane, PC lipids make up a slightly larger proportion of both leaflets of the RBC membrane and POPC makes up the largest portion of PC lipids in the membrane.[15] As such, POPC is a useful model system to study DEHP interactions. After 35 days of storage, 5−10% of DEHP was found to integrate the RBC membrane, resulting in a 5−10% membrane composition.[16] The DEHP concentrations studied in this paper can therefore considered to be physiologically relevant. By studying identical systems in X-ray diffraction experiments and MD simulations, experimental results were comparable and complementary. We determined that DEHP spontaneously partitions into the membrane. It was found to increase membrane thickness and area per lipid and to create a state of increased internal order by increasing lipid tail order and larger-scale disorder by inducing local membrane curvature.

RESULTS

X-ray Diffraction. Diffraction along the membrane normal was measured and is shown in Figure 2. A series of well-developed Bragg peaks are observed as the result of the membrane stacking. The lamellar spacing d_z, i.e., the thickness of the membrane and water layer, is determined from the peak spacing by $d_z = 2\pi/\Delta q_z$. The electron density along the membrane normal, ρ_z, was calculated through Fourier transformation, as described in Materials and Methods.

The electron densities for POPC and for POPC containing 1 and 9 mol % DEHP are shown in Figure 3a. The profiles show a peak in the head group region of the bilayers, where the electron-rich phosphate atoms reside, and a minimum in the

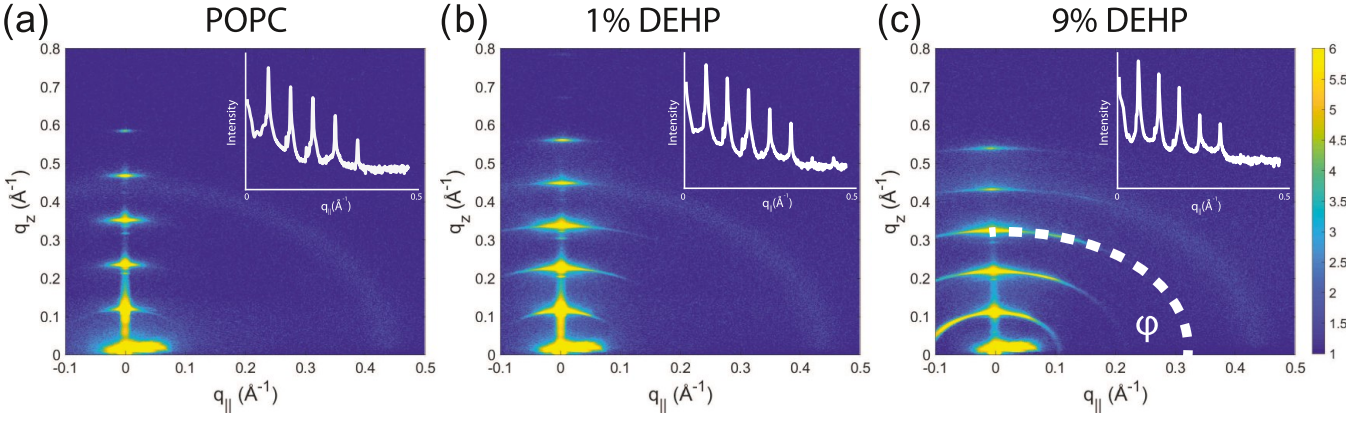

Figure 2. Two-dimensional X-ray intensity maps for pure POPC (a), 1 mol % DEHP:POPC (b), and 9 mol % DEHP:POPC (c). All membrane complexes formed lamellar membranes and lamellar Bragg peaks up to order 5 were used to calculate the electron density profiles. Reflectivity curves were determined by integration and the lamellar peak intensities were determined through fitting of Lorentzian peak profiles. Peak intensities were integrated as a function of the meridional angle, φ, the angle relative to the q_z axis, to determine Hermans orientation function, as sketched in part (c).

https://dx.doi.org/10.1021/acs.langmuir.0c01964
Langmuir 2020, 36, 11899−11907

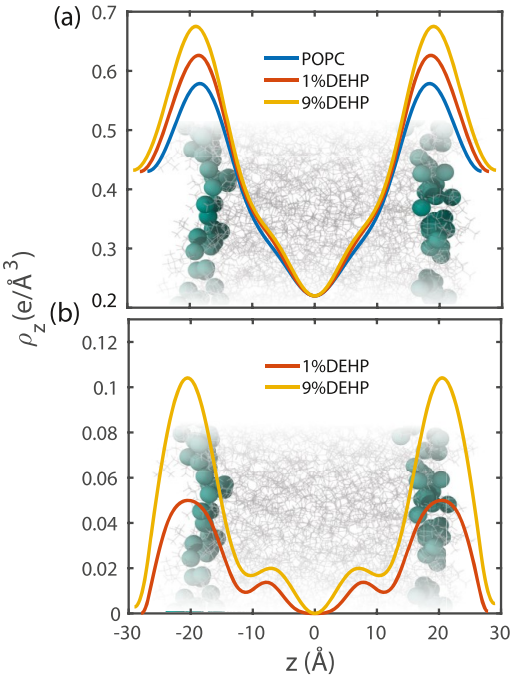

Figure 3. Experimentally determined electron density profiles for pure POPC, 1 mol % DEHP:POPC, and 9 mol % DEHP:POPC. These profiles were found via the reflectivity curves of the hydrated membranes. The different profiles can be attributed to the presence of DEHP in the bilayer (a). Electron density of the DEHP molecules within the bilayers can be determined by subtracting the pure POPC electron density profile from the 1 and 9 mol % membranes' profiles (b).

bilayer center, where only CH_3 groups are found. The membrane width, d_{HH}, was determined from the distance between the two head group maxima. In the presence of DEHP, there is a significant increase in ρ_z, particularly at the head group region of the membranes. Assuming that DEHP alters the membranes' properties only slightly, the position of the DEHP molecules in the membranes can be determined by subtracting the density of the pure POPC bilayers. This is shown in Figure 3b, which plots the difference between the electron density of pure POPC and POPC containing 1 and 9 mol % DEHP.

To model the measured electron density and determine the arrangement of the molecules within the bilayers, the electron density of a DEHP molecule at different tilt angles was calculated and is shown in Figure 4a–c. The calculation utilizes the electronic distribution of each atom of the molecule. To account for thermal motions, a Gaussian distribution, with a half-width of 3.5 Å, is placed at the correct position and all of the atomic contributions are added. The two carbon chains of DEHP can exist in several orientations, therefore the electron density profile of the molecule was calculated in three different molecular orientations: a vertical orientation with the two chains pointing downward and a straddled orientation with the carbon chains pointing outward, representing the two most extreme conformations, and an intermediate position with one vertical and one straddled chain. Once calculated, the electron densities were fitted to those that were experimentally determined in Figure 3b. This was used to locate the position of DEHP in both the 1 and 9% DEHP systems, as indicated in Figure 4d,e. Two main populations of molecules were found: membrane-attached DEHP molecules, which laid flat and were

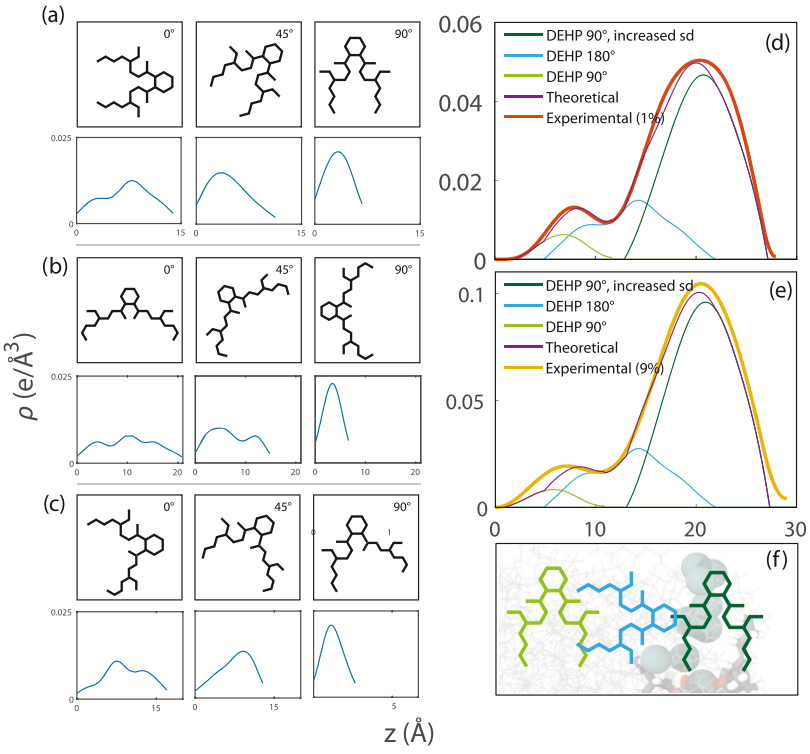

Figure 4. Calculated electron densities of a DEHP molecule at various degrees of rotation in (a). (b) More straddled configuration of the molecule and (c) straddled, however, asymmetric configuration. The corresponding electron densities are sensitive to the structural differences. The calculated electron densities were fitted to the experimental data obtained from the X-ray experiments for the 1% (d) and 9% (e) DEHP:POPC systems. Orientation of the DEHP molecules for the 3 different populations is depicted in part (f).

https://dx.doi.org/10.1021/acs.langmuir.0c01964
Langmuir 2020, 36, 11899−11907

concentrated at the head group region, and DEHP molecules, which had partitioned into the membrane and aligned parallel to the lipid tails. These molecules were located at z-values of 5.2 Å < z < 21.7 Å and their hydrophilic rings pointed toward the head group region, while their hydrophobic tails were embedded within the membrane core. However, the two DEHP populations could not accurately capture the observed experimental density of DEHP in the membranes. A third population of molecules, perpendicular to the lipid tails and close to the center of the bilayer, was therefore tentatively added. Though this population is small, there is evidence of its existence in the complementary MD simulations below. The placement of the DEHP populations in the lipid bilayer is visualized in Figure 4f.

The relative areas under the fitted electron density profiles were used to determine the average partitioning of DEHP into the lipid bilayer. DEHP sitting perpendicularly in the head groups represented 72 and 75% of the total amount of molecules within the low- and high-concentration membranes, respectively. The molecules orienting parallel to the lipid tails represented 23 and 21%, respectively, and the population situated perpendicularly at the membrane core represented 5 and 4% of the total number of molecules in each corresponding membrane system.

DEHP was found to slightly alter membrane width, d_{HH}, and membrane orientation, H, as shown in Figure 5a,b. The presence of DEHP induced a 2% increase in the membrane thickness in a dose-dependent manner, from ∼37 to 38 Å. Simultaneously, membrane orientation decreased with increasing DEHP concentration from ∼96 to 92%. While an orientation value of 100% is indicative of a perfectly flat and rigid membrane, a decrease in the function is a result of the formation of local curvature. We note that although these changes are small, they are well outside the experimental error bars. The experimental errors were determined as follows: Errors for peak positions, peak width, and peak height are determined as the fit standard errors, corresponding to 95% confidence bounds, equivalent to 2 standard deviations, σ. Errors for calculated parameters, such as peak area, were then calculated by applying the proper error propagation.

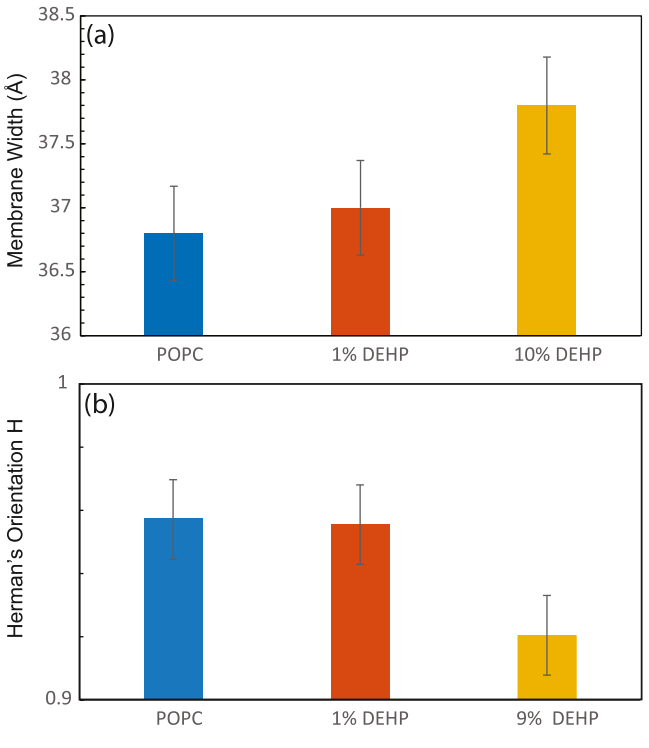

Figure 5. Membrane widths (a) and Hermans orientation function values (b) of the pure POPC, 1 mol % DEHP:POPC, and 9 mol % DEHP:POPC systems, as determined from the experimental electron density profiles and the diffuse circular scattering. All membranes were found to be highly oriented, regardless of their DEHP concentration.

Molecular Dynamics Simulations. Simulations were composed of 128 POPC lipids with either a low (1 mol %) or a high (9 mol %) concentration of DEHP at a hydration of 25 water molecules per lipid molecule. This number of water molecules was determined as the hydration state of the membranes in the experiments and used for better comparison between experiments and simulations. Snapshots of the simulations at different times are shown in Figure 6. In both simulations, DEHP is first observed to spontaneously attach to the bilayer surface, before partitioning and localizing in the center of the membrane. The speed at which this occurs varies with the amount of DEHP added to the system. At low concentrations, Figure 6a, DEHP adsorbs to the upper leaflet surface within 1 ns and finally stabilizes between the leaflets ∼245 ns later. During this time, it is observed to enter a "tug of war" match with the lipid head layer. DEHP is lipid-like in structure, consisting of mostly two nonpolar carbon chains and functional groups near the head area, which give rise to its polarity. At low concentrations, this lipophilic area interacts with the head groups, resulting in its struggle before penetrating fully into the bilayer. Only the molecule added to the upper leaflet was observed to insert into the membrane completely, while the other molecule remained in its tug of war for the duration of the simulation time. Throughout the simulation, both molecules were preferentially positioned with their functional groups directed at the lipid head groups and their carbon tails aligned with bilayer's tails in the hydrophobic region of the membrane. At high concentrations, in Figure 6b, in addition to its adsorption to the bilayer, DEHP molecules aggregated on the surface at 30 ns leading to a distortion in the head group layer, before spontaneously inserting at 33 ns. Dissolution of this cluster occurs gradually. Once fully separated at 186 ns, the molecules exhibit behavior observed in the low-concentration system, with each individual molecule entering their own tug of war before localization within the center of the bilayer.

Electron density profiles of the last 50 ns of the simulations were calculated for the two systems to consolidate the experimentally determined molecular positions. There is a slight expansion in the plots corresponding to increasing DEHP concentration, as observed between Figure 7a,b, in agreement with the increase in membrane width observed in the experimental data. DEHP forms the remaining residual electron density and is observed to localize near the hydrophobic tail group region, at ∼10 Å, seen in Figure 7c,d.

The deuterium order parameter, S_{CD}, and the area per lipid, A_L, were calculated from the simulations. S_{CD} is an indicator of internal membrane order and is calculated by measuring the variance in the orientation, i.e., the mobility, of the C−H bonds within the acyl chains with respect to the bilayer normal.[17] $|S_{CD}|$ of the sn_1 chain for the pure POPC membrane, as well as the two DEHP:POPC membrane systems, is compared in Figure 8a. The presence of DEHP resulted in an

https://dx.doi.org/10.1021/acs.langmuir.0c01964
Langmuir 2020, 36, 11899−11907

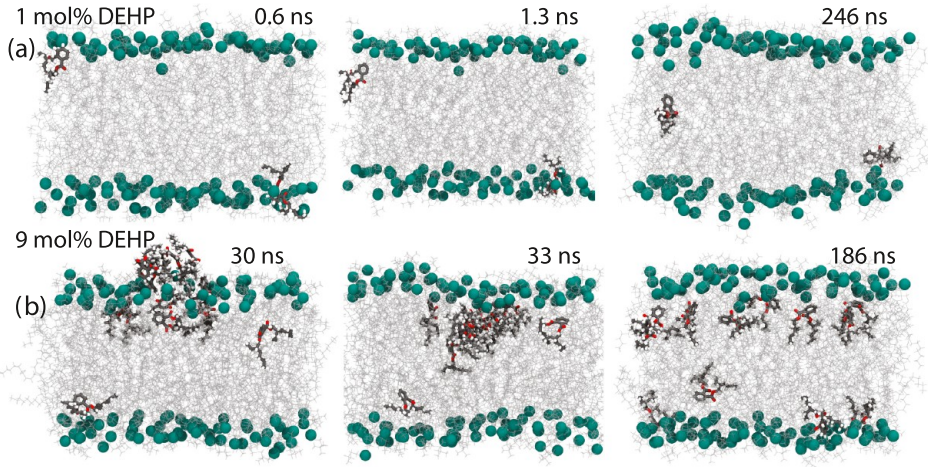

Figure 6. Snapshots of the MD simulations of 128 POPC lipid membranes with low (1 mol %) (a) and high (b) (9 mol %) DEHP concentrations at three different time windows: initial penetration, insertion, and localization. DEHP is observed to spontaneously partition into the bilayers and stabilize at the upper−lower leaflet interface. At high concentrations, DEHP molecules aggregate at the head group layer before subsequent insertion.

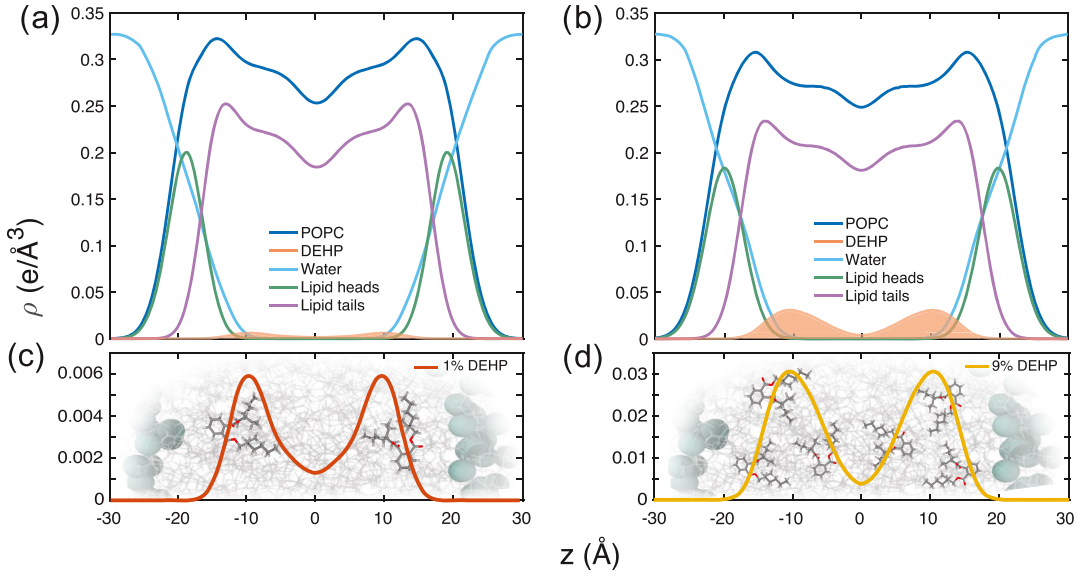

Figure 7. Electron density profiles of 1 mol % (a) and 9 mol % (b) DEHP:POPC membrane systems showing the position of DEHP within the bilayer. Magnifications of these results can be seen in (c) and (d) for low and high concentrations, respectively.

increase in the order parameter for the high concentrations of DEHP, indicating a stiffening of lipid tails in the 9 mol % DEHP:POPC system. A decrease in the order parameters for the low-concentration system was also observed. The area per lipid, Figure 8b, increased monotonically with the amount of DEHP in the bilayers, from 65.8 to 66.3 Å and 69.3 Å.

Figure 8c shows a two-dimensional height map of the simulations in Figure 6. No significant change in height was observed at the beginning of the simulation, while the DEHP molecule was attached to the lipid head groups during the first 5 ns. Once the DEHP is embedded into the membrane core (between 245 and 250 ns), however, the membrane showed a ∼10% increase in height at the position of the embedded DEHP molecule.

DISCUSSION

As a general comment, all effects of DEHP on the structural parameters of the membranes were small, in the order of a few percent, only. They can only be observed when using high-resolution techniques. As such, DEHP is not a disruptive membrane agent and is not expected to induce membrane damage, even at elevated concentrations. While its effects on membrane thickness, area per lipid molecule, lipid and membrane order are subtle, their combination leads to a change in the state of the membranes, which may well have physiological consequences.

By incorporating into the hydrophobic membrane core, DEHP increased the area per lipid. In addition, the membrane width increased, likely as a result of an increase in the order of the lipid tails, as determined from the deuterium order parameters in the MD simulations. DEHP thus makes lipid membranes thicker and less fluid. However, while stiffer membranes typically show an increase in membrane order and lead to "flatter membranes", membrane orientation was found to decrease, indicative of the formation of local membrane curvature.

https://dx.doi.org/10.1021/acs.langmuir.0c01964
Langmuir 2020, 36, 11899−11907

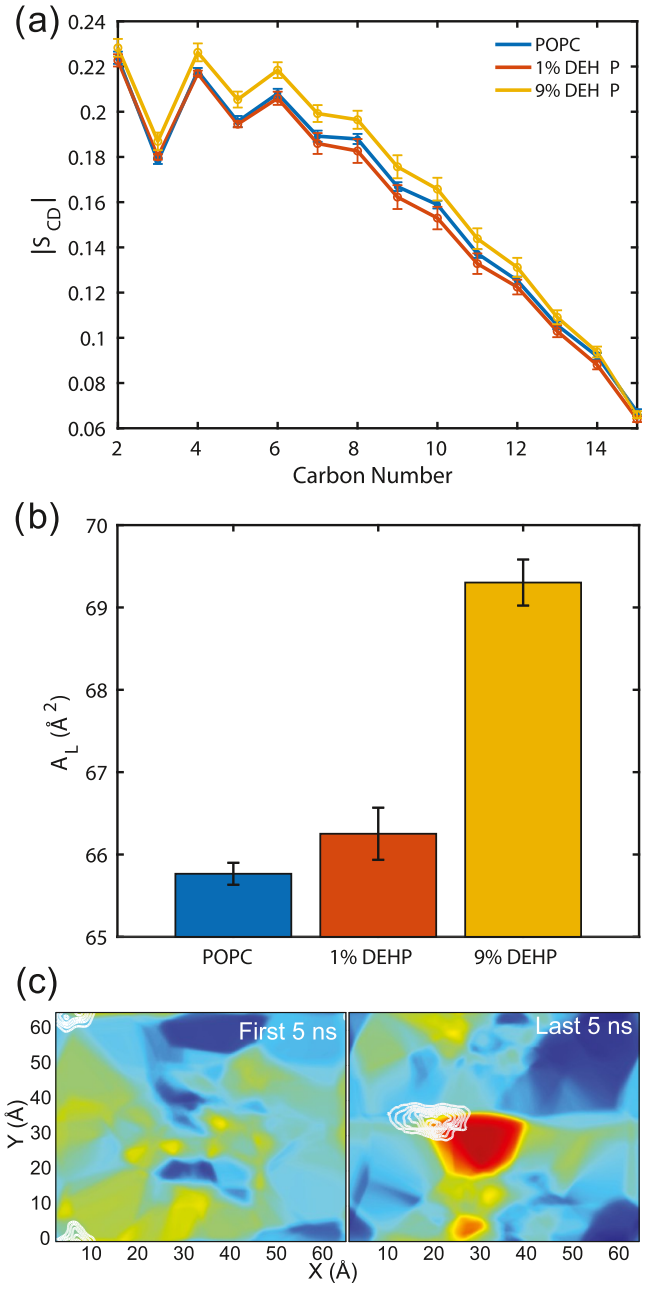

Figure 8. (a) Deuterium order parameters for the sn_1 chain of POPC at low and high concentrations of DEHP as a function of the carbon atom index, with the error bars representing one standard error of the mean (n = 5). (b) Comparison of the area per lipid (A_L) between each of the bilayer systems. The error bars represent one standard error of the mean (n = 5). (c) Two-dimensional height map of the simulations in Figure 6 at 5 ns, with the DEHP attached to the lipid head groups, and at 245 ns, with the DEHP embedded in the membrane core. The membrane shows a 10% increase in height at the position of the embedded DEHP molecule (marked by the white lines).

The mechanism behind the curvature formation can qualitatively be described. The polar groups of the DEHP molecules residing in or just below the lipid head groups slightly repel the lipid tails, thereby separating the head groups and inducing a small convex curvature, as seen with the upper DEHP molecule in the MD snapshot in Figure 6a at 246 ns. A corresponding increase in membrane height is observed in the two-dimensional height map in Figure 8c. Though DEHP's presence in the lipid membrane increases the overall area per lipid, these local changes can tentatively be responsible for increased curvature in the membrane and consequential decrease of Hermans orientation function. The interpretation of these findings is summarized in Figure 9.

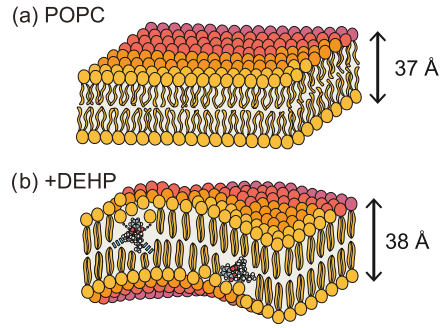

Figure 9. Summary of the findings from X-ray diffraction and MD simulations. DEHP partitions in the lipid membranes and leads to a thickening of the bilayers, an increase of the area per lipid, and the stiffness of the lipid tails. At the same time, it was found to induce local curvature.

There is a large body of literature investigating the effect of DEHP on stored blood. Myhre et al. found that when storing blood, tri-(2-ethylhexyl)trimellitate (TOTM) plasticizers, which is 100 times less leachable as compared to DEHP, RBCs had significantly lower survival rates. Indeed, RBCs had a survival rate below 62.9% (19.5% uncertainty) during a 35 day storage, a decrease from DEHP, which had a 75.3% survival rate (16.7% uncertainty). Blood stored with a DEHP plasticizer also had 20 times more RBCs with regular morphology compared to TOTM.[18] Similarly, Horwitz et al. found that blood cells stored for 21 days at 4 °C in EEA without DEHP compared to PVC (approximately 40% DEHP) showed higher percentages of osmotic fragility, 20 ± 9% compared to 3 ± 2%, and higher concentrations of hemoglobin in plasma 109 ± 54 mg/dL compared to 31 ± 19 mg/dL. Recent research reported that DINCH (1,2-cyclohexane dicarboxylic acid diisononyl ester)-PVC blood bags are a possible alternative of DEHP-PVC blood bags. DINCH-PVC blood bags showed higher rates of hemolysis in static storage. However, hemolysis levels were equal to those in DEHP blood bags when the blood stored in DINCH was mixed weekly during the 42 day storage time.[19,20] Another study by Lagerberg et al. found that RBCs stored in DINCH alone had higher rates of hemolysis, while additional additive solutions to the DINCH blood bags lowered hemolysis to a rate similar to that of DEHP and that DINCH was shown to be 10-fold less leachable compared to DEHP.[21] Similar results were obtained by Högman et al. when using butyryl-n-trihexyl-citrate (BTHC) as a substitute to DEHP. BTHC was less leachable and achieved hemolysis levels comparable to DEHP only when regularly mixed throughout the storage time.[22]

These studies suggest that DEHP's ability to leach into the blood and interact with RBCs is key to lowering the hemolysis rates. It has long been speculated that the DEHP molecules partition in the cell membranes of the RBCs and change the membrane properties.[23] Though the exact mechanism is unknown, it has been theorized that aging RBC membranes loose flexibility due to a changing cholesterol to lipid ratio.

https://dx.doi.org/10.1021/acs.langmuir.0c01964
Langmuir 2020, 36, 11899−11907

DEHP may fill in space, allowing the RBC to maintain its structure. This property would be unique to DEHP, as most plasticizers do not integrate the membrane.[3] Our analysis of DEHP partitioning and membrane effects supports these findings. As DEHP integrates the membrane, it increases membrane rigidity and thickness, leading to a subsequent increase in stability. With populations existing both in the head groups and tails, DEHP can likely fill in the membrane gaps formed by changing the lipid ratios and provide subsequent membrane stability.

CONCLUSIONS

We studied the interaction between the DEHP and POPC membranes using X-ray diffraction and MD simulations. At low concentrations, DEHP spontaneously partitioned in the lipid bilayers, while at high concentrations, the molecules formed an aggregate before insertion and eventual dissolution. The molecules were located in three different populations. Most molecules localized in the head group region, aligning parallel to the membranes (~72%). A smaller fraction (~23%) was found aligned parallel to the lipid tails, beneath the head groups. Another small population (~5%) localized near the center of the bilayer. DEHP was observed to increase membrane width and its area per lipid. An increase in local membrane curvature indicates lower membrane order, while the deuterium order parameter was found to slightly increase, suggesting a stiffening of the lipid tails. These findings suggest that DEHP creates thicker, more rigid membranes, with a slightly corrugated surface morphology. These results could explain the increased stability of RBCs, due to the lower rates of hemolysis and improved aging morphology, when stored in the DEHP-based blood bags.

MATERIALS AND METHODS

Membrane Preparation. Highly oriented multilamellar membranes were prepared on single-side polished silicon wafers. 1-Palmitoyl-2-oleoyl-*sn*-glycero-3-phosphocholine (POPC, Avanti Polar Lipids) and bis(2-ethylhexyl)phthalate (DEHP, Sigma) were mixed at the desired molecular ratio and dissolved in a 1:1 mixture of chloroform (Caledon) and 2,2,2-trifluoroethanol (TFE) (Sigma). The final solution concentration was 15 mg/mL.

The wafers were placed in 1,2-dichloromethane (Caledon) within a closed Pyrex dish. The wafers were cleaned by sonication for 30 min, which resulted in a hydrophobic silicon surface. The wafers were then removed and rinsed three times thoroughly with alternating methanol and ultrapure (18.2 Ω·cm) water. The wafers were then dried with pressurized nitrogen gas and placed on a tilting incubator set to 310 K. A syringe was used to deposit ~80 μL of the POPC-DEHP solution on the wafer while the tilt (speed 15, tilt angle 1°) provided circular flow and even distribution. The samples were allowed to dry for 20 min on the tilting incubator.

The samples were placed in vacuum for ~12 h at 298 K to allow for the evaporation of trace solvent and subsequently annealed at 310 K in a K_2SO_4 atmosphere at 98% relative humidity for ~12 h.

X-ray Diffraction Experiment. X-ray scattering data was obtained using the Biological Large Angle Diffraction Experiment (BLADE) in the Laboratory for Membrane and Protein Dynamics at McMaster University. BLADE uses a 9 kW (45 kV, 200 mA) Cu Kα rotating anode at a wavelength of 1.5418 Å using a Rigaku HyPix-3000 2D semiconductor detector with an area of 3000 mm^2 and 100 μm pixel size.[24] All samples were prepared and measured in replicates to check for consistency. Both source and detector are mounted on movable arms such that the membranes stay horizontal during the measurements. Focusing multilayer optics provides a high-intensity parallel beam of ~200 μm with monochromatic X-ray intensities of up to 10^8 counts. Note that there is no risk of sample damage using this in-house technique because of the relatively low intensity of the X-ray beam as compared to the synchrotron sources. The samples were mounted in a custom-built humidity chamber during the experiments to control the humidity of the membranes.

The result of an X-ray experiment is a two-dimensional intensity map of a large area of the reciprocal space, as sketched in Figure 2. All scans were measured at 30 °C and 98% relative humidity in a K_2SO_4 atmosphere to ensure hydration of the membranes.

The out-of-plane structure of the membrane was determined using specular reflectivity. The relative electron density, $\rho(z)$, can be approximated by a one-dimensional Fourier analysis.[25]

$$\rho(z) = \frac{2}{d_z}\sum_{n=1}^{N} F(q_n)\nu_n \cos(q_n z) = \frac{2}{d_z}\sum_{n=1}^{N} \sqrt{I_n q_n}\,\nu_n \cos\left(\frac{2\pi n z}{d_z}\right) \quad (1)$$

where N is the highest order of the Bragg peaks observed. $F(q_n)$ is the form factor and is determined by multiplying the integrated peak intensity I_n with q_n[25] and is in general a complex quantity. In the case of centrosymmetry, the form factor becomes real and the phase problem of crystallography, therefore, simplifies to the sign problem $F(q_z) = \pm|F(q_z)|$. An X-ray diffraction experiment probes the form factor at discrete values of q_z, and a continuous function, $T(q_z)$ (proportional to the bilayer form factor), can be fitted to the data[25]

$$T(q_z) = \sum_n \sqrt{I_n q_n}\ \mathrm{sinc}\left(\frac{1}{2}d_z q_z - \pi n\right) \quad (2)$$

Once an analytical expression for $T(q_z)$ has been determined from fitting the experimental peak intensities, the phases ν_n can be assessed from $T(q_z)$. The phase array $\nu_n = [-1\ -1\ 1\ -1\ 1]$ was used for all samples.

$\rho(z)$ is initially calculated on an arbitrary scale, it is then scaled based on the protocol established in our previous work.[26] The curves are scaled until the total number of electrons within the lipid unit cell across a membrane leaflet $e^- = A_L\int_0^{d_z/2}\rho(z)dz$ agrees with the total number of electrons expected based on the sample composition. $\rho(z)$ was scaled by the number of electrons per unit cell, including the electron contributions from the membrane lipids, DEHP, and water, while the bilayer core z = 0 Å was fixed at 0.22 $e^-/Å^3$ to represent terminal methyl groups of the lipid acyl chain.

To determine the degree of orientation of the membranes in the stack, the correlation peak intensities were integrated as a function of the meridional angle φ (the angle relative to the q_z axis, as sketched in Figure 2c). The corresponding intensity was fit with a Gaussian distribution centered at 0, which was then used to calculate the degree of orientation using Hermans orientation function

$$H = \frac{3 < \cos^2\delta > -1}{2} \quad (3)$$

H = 1.0 corresponds to lipids, which are perfectly parallel to each other within the bilayer (hyperordered), whereas H = 0.25 corresponds to a membrane with lipids in complete disorder.

Molecular Dynamics Simulations. Atomistic membrane simulations were conducted with GROMACS 5.1.4 on MacSim, a GPU accelerated computer workstation.[27] This computer is equipped with a 40 Core central processing unit (CPU, Intel(R) Xeon(R) CPU E5-2630 v4 @ 2.20GHz), 130 GB random-access memory (RAM), and three graphic processing units (GPU, 2 NVIDIA 1080 TDI + 1 GeForce GT 730). The simulations used the Stockholm lipids (Slipids) force field[28] and the simple-point charge (SPC) water model for solvation.[29] The lipid topology for POPC was taken from Jämbeck and Lyubartsev[30,31] and the DEHP topology was constructed using the Amber 16 program Antechamber alongside the general Amber force field (GAFF).[32,33] To determine the interactions between the lipid bilayer and varying amounts of DEHP, three membrane systems of 128 POPC lipids (64 per leaflet) were created using MemGen according to Table 1.[34] DEHP molecules were randomly added

https://dx.doi.org/10.1021/acs.langmuir.0c01964
Langmuir 2020, 36, 11899−11907

Table 1. Listed are the Membrane Composition, the Number of DEHP and Water Molecules[a]

membrane system	n_{DEHP}	n_W
POPC	0	3200
+1 mol % DEHP	2	
+9 mol % DEHP	12	

[a]All simulations were run for 250 ns.

external to the membrane in low (1 mol %) and high (9 mol %) concentrations. The systems were then solvated. The membranes were fully hydrated with 25 water molecules per lipid molecule.

The systems were first energy minimized and then equilibrated using an NVT/NPT ensemble before being simulated for 250 ns. All simulations used a 2 fs time step, a periodic boundary condition applied to all directions, a short-range van der Waals cutoff of 1.2 nm, the particle-mesh Ewald method using a real-space cutoff of 1.2 nm, fourth-order interpolation, and 0.16 nm grid spacing to solve for long-range electrostatics.[35] The parallel LINCS (P-LINCS) algorithm was used to determine bond constraints.[36] Temperature and pressure were maintained at 303 K and 1.0 bar using a Nosé−Hoover thermostat[37−39] at 28 °C (τ = 0.5 ps) and Parrinello−Rahman semi-isotropic weak coupling (τ = 1 ps).[40] All analyses were performed on the last 50 ns of the simulations to ensure that full equilibration had been achieved. Error estimates were calculated using the block averaging approach over five blocks using the full-precision averages.[41] Analysis was carried out using GROMACS algorithms and simple scripts within our library. The electron density profiles of the systems were calculated by generating index files for each membrane component and employing the built-in function gmx density, which computes partial densities along the normal (z) direction of the bilayer.

The deuterium order parameter, S_{CD}, was calculated using

$$S_{CD} = \frac{1}{2}\langle 3\cos^2\theta - 1\rangle \quad (4)$$

where θ is the angle between the C−H bond and the normal. Deuterium order parameters for carbons in the acyl chains of POPC were calculated using the function gmx order. This value is a measure of lipid ordering and is used here as a proxy for lipid rigidity.[42] It should be noted that, by default, this function is unable to calculate the order parameters for terminal carbons, due to their lack of neighboring atoms, so only the values for carbons 2−15 are shown.

Two-dimensional membrane height profiles were generated using the modified GridMAT-MD algorithm from ref 43, provided as GROMACS tool from http://www.mpibpc.mpg.de/groups/de_groot/software.html.

AUTHOR INFORMATION

Corresponding Author

Maikel C. Rheinstädter − *Department of Physics and Astronomy and Origins Institute, McMaster University, Hamilton, Ontario L8S 4M1, Canada;* orcid.org/0000-0002-0558-7475; Phone: +1-(905)-525-9140-23134; Email: rheinstadter@mcmaster.ca; Fax: +1-(905)-546-1252

Authors

Renée-Claude Bider − *Department of Physics and Astronomy and Origins Institute, McMaster University, Hamilton, Ontario L8S 4M1, Canada*

Telmah Lluka − *Department of Physics and Astronomy and Origins Institute, McMaster University, Hamilton, Ontario L8S 4M1, Canada*

Sebastian Himbert − *Department of Physics and Astronomy and Origins Institute, McMaster University, Hamilton, Ontario L8S 4M1, Canada*

Adree Khondker − *Department of Physics and Astronomy and Origins Institute, McMaster University, Hamilton, Ontario L8S 4M1, Canada*

Syed M. Qadri − *Faculty of Health Sciences, Ontario Tech University, Oshawa, Ontario L1G 0C5, Canada*

William P. Sheffield − *Department of Pathology and Molecular Medicine, McMaster University, Hamilton, Ontario L8S 4M1, Canada; Centre for Innovation, Canadian Blood Services, Hamilton, Ontario L8S 4M1, Canada*

Complete contact information is available at: https://pubs.acs.org/10.1021/acs.langmuir.0c01964

Author Contributions

⊥R.-C.B. and T.L. contributed equally to this work.

Notes

The authors declare no competing financial interest.

ACKNOWLEDGMENTS

This research was funded by the Natural Sciences and Engineering Research Council of Canada (NSERC), the Canada Foundation for Innovation (CFI), and the Ontario Ministry of Economic Development and Innovation. M.C.R. is the recipient of an Early Researcher Award of the Province of Ontario and a University Scholar of McMaster University. The funders had no role in study design, data collection and analysis, decision to publish, or preparation of the manuscript.

REFERENCES

(1) Rock, G.; Labow, R. S.; Tocchi, M. Distribution of di(2-ethylhexyl) phthalate and products in blood and blood components. *Environ. Health Perspect.* **1986**, *65*, 309−316.

(2) Rahman, M.; Brazel, C. S. The plasticizer market: An assessment of traditional plasticizers and research trends to meet new challenges. *Prog. Polym. Sci.* **2004**, *29*, 1223−1248.

(3) Simmchen, J.; Ventura, R.; Segura, J. Progress in the removal of di-[2-ethylhexyl]-phthalate as plasticizer in blood bags. *Transfus. Med. Rev.* **2012**, *26*, 27−37.

(4) Heudorf, U.; Mersch-Sundermann, V.; Angerer, J. Phthalates: Toxicology and exposure. *Int. J. Hyg. Environ. Health* **2007**, *210*, 623−634.

(5) Rock, G.; Labow, R. S.; Tocchi, M.; Tickner, J. A.; Schettler, T.; Guidotti, T.; McCally, M.; Rossi, M. Health risks posed by use of di-2-ethylhexyl phthalate (DEHP) in PVC medical devices: A critical review. *Am. J. Ind. Med.* **2001**, *39*, 100−111.

(6) Dhanya, C.; Indu, A.; Deepadevi, K.; Kurup, P. Inhibition of membrane Na^+-K^+ ATPase of the brain, liver and RBC in rats administered di (2-ethyl hexyl) phthalate (DEHP) a plasticizer used in polyvinyl chloride (PVC) blood storage bags. *Indian J. Exp. Biol.* **2003**, *41*, 814−820.

(7) Rael, L. T.; Bar-Or, R.; Ambruso, D. R.; Mains, C. W.; Slone, D. S.; Craun, M. L.; Bar-Or, D. Phthalate esters used as plasticizers in packed red blood cell storage bags may lead to progressive toxin exposure and the release of pro-inflammatory cytokines. *Oxid. Med. Cell. Longevity* **2009**, *2*, 166−171.

(8) Carmen, R. The selection of plastic materials for blood bags. *Transfus. Med. Rev.* **1993**, *7*, 1−10.

(9) Inoue, K.; Kawaguchi, M.; Yamanaka, R.; Higuchi, T.; Ito, R.; Saito, K.; Nakazawa, H. Evaluation and analysis of exposure levels of di (2-ethylhexyl) phthalate from blood bags. *Clin. Chim. Acta* **2005**, *358*, 159−166.

(10) Scientific Opinion on the safety of medical devices containing DEHP-plasticized PVC or other plasticizers on neonates and other groups possibly at risk, 2015. https://op.europa.eu/en/publication-detail/-/publication/1bee9152-0253-11e7-8a35-01aa75ed71a1/language-en.

(11) Holme, S. Current issues related to the quality of stored RBCs. *Transfus. Apher. Sci.* **2005**, *33*, 55−61.
(12) Rock, G.; Tocchi, M.; Ganz, P. R.; Tackaberry, E. S. Incorporation of plasticizer into red cells during storage. *Transfusion* **1984**, *24*, 493−498.
(13) Almizraq, R.; Tchir, J. D. R.; Holovati, J. L.; Acker, J. P. Storage of red blood cells affects membrane composition, microvesiculation, and in vitro quality. *Transfusion* **2013**, *53*, 2258−2267.
(14) Melzak, K. A.; Uhlig, S.; Kirschhöfer, F.; Brenner-Weiss, G.; Bieback, K. The blood bag plasticizer di-2-ethylhexylphthalate causes red blood cells to form stomatocytes, possibly by inducing lipid flip-flop. *Transfus. Med. Hemother.* **2018**, *45*, 413−422.
(15) Himbert, S.; Blacker, M. J.; Kihm, A.; Pauli, Q.; Khondker, A.; Yang, K.; Sinjari, S.; Johnson, M.; Juhasz, J.; Wagner, C.; Stöver, H. D. H.; Rheinstädter, M. C. Hybrid Erythrocyte Liposomes: Functionalized Red Blood Cell Membranes for Molecule Encapsulation. *Adv. Biosyst.* **2020**, *4*, No. 1900185.
(16) Farquhar, J. W.; Ahrens, E. H. Effects of dietary fats on human erythrocyte fatty acid patterns. *J. Clin. Invest.* **1963**, *42*, 675−685.
(17) Piggot, T. J.; Allison, J. R.; Sessions, R. B.; Essex, J. W. On the calculation of acyl chain order parameters from lipid simulations. *J. Chem. Theory Comput.* **2017**, *13*, 5683−5696.
(18) Myhre, B. A.; Johnson, D.; Marcus, C. S.; Demaniew, S.; Carmen, R.; Nelson, E. Survival of red cells stored for 21 and 35 days in a non-di-(2-ethylhexyl) phthalate plastic container. *Vox Sang.* **1987**, *53*, 199−202.
(19) Gulliksson, H.; van der Meer, P. F. Storage of whole blood overnight in different blood bags preceding preparation of blood components: In vitro effects on red blood cells. *Blood Transfus.* **2009**, *7*, 210.
(20) Dumont, L. J.; Baker, S.; Dumont, D. F.; Herschel, L.; Waters, S.; Calcagni, K.; Sandford, C.; Radwanski, K.; Min, K.; David, R. M.; et al. Exploratory in vitro study of red blood cell storage containers formulated with an alternative plasticizer. *Transfusion* **2012**, *52*, 1439−1445.
(21) Lagerberg, J. W.; Gouwerok, E.; Vlaar, R.; Go, M.; de Korte, D. In vitro evaluation of the quality of blood products collected and stored in systems completely free of di (2-ethylhexyl) phthalate-plasticized materials. *Transfusion* **2015**, *55*, 522−531.
(22) Högman, C. F.; Eriksson, L.; Ericson, Å.; Reppucci, A. J. Storage of saline-adenine-glucose-mannitol-suspended red cells in a new plastic container: Polyvinylchloride plasticized with butyryl-n-trihexyl-citrate. *Transfusion* **1991**, *31*, 26−29.
(23) Horowitz, B.; Stryker, M. H.; Waldman, A. A.; Woods, K. R.; Gass, J. D.; Drago, J. Stabilization of Red Blood Cells by the Plasticizer, Diethylhexylphthalate 1. *Vox Sang.* **1985**, *48*, 150−155.
(24) Khondker, A.; Malenfant, D. J.; Dhaliwal, A. K.; Rheinstädter, M. C. Carbapenems and lipid bilayers: Localization, partitioning, and energetics. *ACS Infect. Dis.* **2018**, *4*, 926−935.
(25) Nagle, J. F.; Wiener, M. C. Relations for lipid bilayers. Connection of electron density profiles to other structural quantities. *Biophys. J.* **1989**, *55*, 309−313.
(26) Alsop, R. J.; Khondker, A.; Hub, J. S.; Rheinstädter, M. C. The Lipid Bilayer Provides a Site for Cortisone Crystallization at High Cortisone Concentrations. *Sci. Rep.* **2016**, *6*, No. 22425.
(27) Abraham, M. J.; Murtola, T.; Schulz, R.; Páll, S.; Smith, J. C.; Hess, B.; Lindahl, E. GROMACS: High performance molecular simulations through multi-level parallelism from laptops to supercomputers. *SoftwareX* **2015**, *1−2*, 19−25.
(28) Jämbeck, J. P. M.; Lyubartsev, A. P. Derivation and Systematic Validation of a Refined All-Atom Force Field for Phosphatidylcholine Lipids. *J. Phys. Chem. B* **2012**, *116*, 3164−3179.
(29) Berendsen, H. J.; Postma, J. P.; van Gunsteren, W. F.; Hermans, J. Interaction models for water in relation to protein hydration. *Annu. Rep. Comput. Chem.* **1981**, 331−342.
(30) Jämbeck, J. P. M.; Lyubartsev, A. P. An Extension and Further Validation of an All-Atomistic Force Field for Biological Membranes. *J. Chem. Theory Comput.* **2012**, *8*, 2938−2948.
(31) Jämbeck, J. P. M.; Lyubartsev, A. P. Another piece of the membrane puzzle: Extending slipids further. *J. Chem. Theory Comput.* **2013**, *9*, 774−784.
(32) Wang, J.; Wolf, R. M.; Caldwell, J. W.; Kollman, P. A.; Case, D. A. Development and testing of a general Amber force field. *J. Comput. Chem.* **2004**, *25*, 1157−1174.
(33) Wang, J.; Wolf, R. M.; Caldwell, J. W.; Kollman, P. A.; Case, D. A. Erratum: Development and testing of a general Amber force field. *J. Comput. Chem.* **2005**, *26*, 1157−1174.
(34) Knight, C. J.; Hub, J. S. MemGen: A general web server for the setup of lipid membrane simulation systems. *Bioinformatics* **2015**, *31*, 2897−2899.
(35) Darden, T.; York, D.; Pedersen, L. Particle mesh Ewald: An N·log(N) method for Ewald sums in large systems. *J. Chem. Phys.* **1993**, *98*, 10089−10092.
(36) Hess, B. P-LINCS: A parallel linear constraint solver for molecular simulation. *J. Chem. Theory Comput.* **2008**, *4*, 116−122.
(37) Nosé, S. A molecular dynamics method for simulations in the canonical ensemble. *Mol. Phys.* **1984**, *52*, 255−268.
(38) Nosé, S. A unified formulation of the constant temperature molecular dynamics methods. *J. Chem. Phys.* **1984**, *81*, 511−519.
(39) Hoover, W. G. Canonical dynamics: Equilibrium phase-space distributions. *Phys. Rev. A* **1985**, *31*, 1695−1697.
(40) Parrinello, M.; Rahman, A. Polymorphic transitions in single crystals: A new molecular dynamics method. *J. Appl. Phys.* **1981**, *52*, 7182−7190.
(41) Piggot, T. J.; Allison, J. R.; Sessions, R. B.; Essex, J. W. Quantifying uncertainty and sampling quality in biomolecular simulations. *Intermol. Forces* **1981**, *5*, 23−48.
(42) Gapsys, V.; de Groot, B. L.; Briones, R. Computational analysis of local membrane properties. *J. Comput.-Aided Mol. Des.* **2013**, *27*, 845−858.
(43) Gapsys, V.; de Groot, B. L.; Briones, R. Computational analysis of local membrane properties. *J. Comput.-Aided Mol. Des.* **2013**, *27*, 845−858.

https://dx.doi.org/10.1021/acs.langmuir.0c01964
Langmuir 2020, 36, 11899−11907